CHEMISTRY OF MATERIALS
Article

Chem. Mater. **2009,** *21,* 4759–4767 4759
DOI:10.1021/cm802850s

Self-Organized Growth of Organic Thiophene−Phenylene Nanowires on Silicate Surfaces

Frank Balzer,*,† Manuela Schiek,*,† Arne Lützen,‡ and Horst-Günter Rubahn†

†*Mads Clausen Institute, NanoSYD, University of Southern Denmark, Alsion 2, DK-6400 Sønderborg, Denmark, and* ‡*Kekulé-Institute of Organic Chemistry and Biochemistry, University of Bonn, Gerhard-Domagk-Strasse 1, D-53121 Bonn, Germany*

Received October 20, 2008. Revised Manuscript Received September 2, 2009

Results of a systematic study of the growth of blue-green light-emitting 2,5-di-4-biphenyl-thiophene (PPTPP) molecules on the (001) faces of the sheet silicates muscovite and phlogopite mica are reported. This includes morphology, crystallography, and optical properties. It is shown that small changes in the choice of the substrate lead to distinctly different growth behavior. On muscovite, a commensurate wetting layer of lying molecules is initially formed with subsequent formation of clusters, which assemble into mutually parallel nanowires. The wires grow along a ⟨110⟩ muscovite direction, having the molecules oriented perpendicular to the wire direction and parallel to the surface plane. On phlogopite mica, no wetting layer is observed, but diffraction from islands of upright molecules, forming a coincidence lattice. Fibers grow along three different directions, until they start bending. In comparison to similar organic molecules, it is found that overall PPTPP has a growth behavior more similar to that of the *p*-phenylenes as compared to that of the α-thiophenes.

Introduction

Light-emitting organic nanowires (or "nanofibers", "needles") have evolved as a very active research field during the last years.[1,2] Waveguiding,[3] lasing,[4] electrical transport,[5,6] mechanical properties,[7] and nonlinear optics[8−10] have been investigated. The organic aggregates have either been grown directly on surfaces by organic molecular beam deposition and by hot wall epitaxy,[11] by solvent vapor annealing,[12] or they have been assembled in solution and then deposited onto a surface.[13−16] The formation of upright nanowires on a substrate has been facilitated by, for example, filling of mesoporous substrates[17,18] or even by vapor phase deposition.[19,20]

The most detailed experimental data exist for organic molecular beam deposition and for hot-wall epitaxy of *p*-hexaphenylene (*p*-6P) on various substrate surfaces.[21,22] Sheet silicates such as micas are known to promote uniaxial growth.[23−26] On muscovite mica, for example, *p*-6P forms clusters as well as mutually parallel nanofibers from lying molecules, the fibers growing mainly by cluster aggregation. The first step in the growth process is the formation of a wetting layer from lying molecules.[27] The wetting layer is crystalline, resulting in a well-defined

*To whom correspondence should be addressed. E-mail: fbalzer@mci.sdu.dk (F.B.); schiek@mci.sdu.dk (M.S.).

(1) Schiek, M.; Balzer, F.; Al-Shamery, K.; Brewer, J.; Lützen, A.; Rubahn, H.-G. *Small* **2008**, *4*, 176–181.
(2) Schiek, M.; Balzer, F.; Al-Shamery, K.; Lützen, A.; Rubahn, H.-G. *Soft Matter* **2008**, *4*, 277–285.
(3) Zhao, Y.; Xu, J.; Peng, A.; Fu, H.; Ma, Y.; Jiang, L.; Yao, J. *Angew. Chem., Int. Ed.* **2008**, *47*, 7301–7305.
(4) Quochi, F.; Cordella, F.; Mura, A.; Bongiovanni, G.; Balzer, F.; Rubahn, H.-G. *J. Phys. Chem. B* **2005**, *109*, 21690–21693.
(5) Kjelstrup-Hansen, J.; Henrichsen, H.; Bøgild, P.; Rubahn, H.-G. *Thin Solid Films* **2006**, *515*, 827–830.
(6) Briseno, A.; Mannsfeld, S.; Reese, C.; Hancock, J.; Xiong, Y.; Jenekhe, S.; Bao, Z.; Xia, Y. *Nano Lett.* **2007**, *7*, 2847–2853.
(7) Kjelstrup-Hansen, J.; Hansen, O.; Rubahn, H.-G.; Bøggild, P. *Small* **2006**, *2*, 660–666.
(8) Brewer, J.; Schiek, M.; Lützen, A.; Al-Shamery, K.; Rubahn, H.-G. *Nano Lett.* **2006**, *6*, 2656–2659.
(9) Brewer, J.; Schiek, M.; Wallmann, I.; Rubahn, H.-G. *Opt. Commun.* **2008**, *281*, 3892–3896.
(10) Quochi, F.; Saba, M.; Cordella, F.; Gocalinska, A.; Corpino, R.; Marceddu, M.; Anedda, A.; Andreev, A.; Sitter, H.; Sriciftci, N.; Mura, A.; Bongiovanni, G. *Adv. Mater.* **2008**, *20*, 3017–3021.
(11) *Organic Nanostructures for Next Generation Devices*; Al-Shamery, K., Rubahn, H.-G., Sitter, H., Eds.; Springer Series in Materials Science; Springer: Berlin, 2008; Vol. *101*.
(12) Mascaro, D.; Thompson, M.; Smith, H.; Bulovic, V. *Org. Electron.* **2005**, *6*, 211–220.
(13) Wang, Z.; Ho, K.; Medforth, C.; Shelnutt, J. *Adv. Mater.* **2006**, *18*, 2557–2560.
(14) Briseno, A.; Mannsfeld, S.; Lu, X.; Xiong, Y.; Jenekhe, S.; Bao, Z.; Xia, Y. *Nano Lett.* **2007**, *7*, 668–675.
(15) Kim, D.; Lee, D.; Lee, H.; Lee, W.; Kim, Y.; Han, J.; Cho, K. *Adv. Mater.* **2007**, *19*, 678–682.
(16) Mille, M.; Lamere, J.-F.; Rodrigues, F.; Fery-Forgues, S. *Langmuir* **2008**, *24*, 2671–2679.
(17) O'Carroll, D.; Lieberwirth, I.; Redmond, G. *Small* **2007**, *3*, 1178–1183.
(18) Moynihan, S.; Iacopino, D.; O'Carroll, D.; Lovera, P.; Redmond, G. *Chem. Mater.* **2008**, *20*, 996–1003.
(19) Zhao, Y.; Xiao, D.; Yang, W.; Peng, A.; Yao, J. *Chem. Mater.* **2006**, *18*, 2302–2306.
(20) Chung, J.; An, B.-K.; Kim, J.; Kim, J.-J.; Park, S. *Chem. Comm.* **2008**, 2998–3000.
(21) Kankate, L.; Balzer, F.; Niehus, H.; Rubahn, H.-G. *J. Chem. Phys.* **2008**, *128*, 084709.
(22) Resel, R. *J. Phys.: Condens. Matter* **2008**, *20*, 184009.
(23) Uyeda, N.; Ashida, M.; Suito, E. *J. Appl. Phys.* **1965**, *36*, 1453–1460.
(24) Ashida, M. *Bull. Chem. Soc. Jpn.* **1966**, *39*, 2625–2631.
(25) Kobzareva, S.; Distler, G. *J. Cryst. Growth* **1971**, *10*, 269–275.
(26) Sun, M.; Stetco, A.; Merschrod, S., E. *Langmuir* **2008**, *24*, 5418–5421.
(27) Frank, P.; Hlawacek, G.; Lengyel, O.; Satka, A.; Teichert, C.; Resel, R.; Winkler, A. *Surf. Sci.* **2007**, *601*, 2152–2160.

Published on Web 09/28/2009

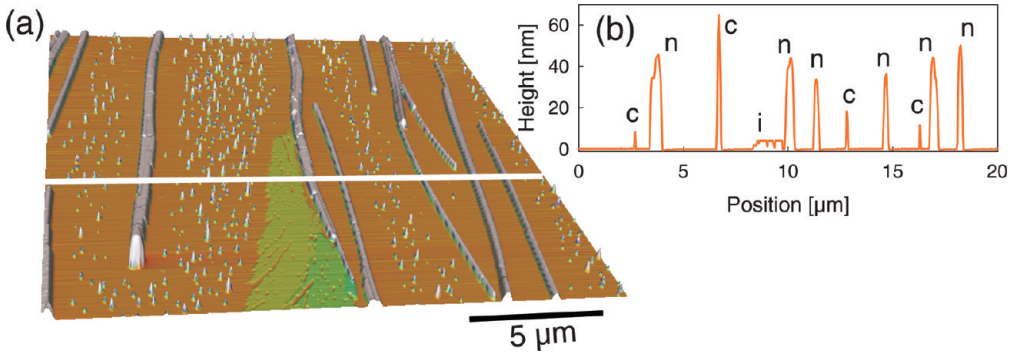

Figure 1. (a) AFM image, $20 \times 20\,\mu m^2$, of 7.5 nm PPTPP deposited on muscovite mica at a substrate temperature of $T_S = 370$ K, demonstrating the overall morphology. (b) Cross-section through the image (white line in a), depicting typical heights of the needles ("n"), flat islands ("i"), and clusters (all other peaks).

low-energy electron diffraction (LEED) pattern.[28] On other substrates such as KCl, a wetting layer has not been observed, although similar needles grow.[29] Similarly, for other conjugated molecules such as α-quaterthiophene and α-sexithiophene on muscovite, no wetting layer has been detected by LEED, yet.[30]

Besides phenylenes and thiophenes, another class of interesting molecules are the phenylene/thiophene co-oligomers because of their fortunate optical and electrical properties.[31−34] Field-effect transistors,[32] amplified spontaneous emission,[35] and lasing[36,37] have been demonstrated. However, it is well-known that oriented nanofiber formation is restricted to certain combinations of organic molecules and growth substrates. Therefore, both from a fundamental point of view as well as from the application side, it is of interest to study the formation of thin films from thiophene/phenylene co-oligomers on dielectric surfaces. Choosing different sequences and numbers of thiophene and phenylene rings, molecules more thiophene- or more phenylene-like can be tested. Different shapes such as zigzag or bananalike allow the exploration of structure−property relationships.[38,39] Reports about the overall morphology of thin films grown from the zigzag-like co-oligomers 5,5′-di-4-biphenyl-2,2′-bithiophene (PPTTPP) and 4,4′-di-2,2′-bithienyl-biphenyl (TTPPTT) already exist.[40] On muscovite mica, they form nanowires, growing simultaneously along two or more different directions, thus limiting the maximal length but resulting in meshlike structures.[41] In this paper we will investigate in more detail the formation of thin films from the banana-shaped 2,5-di-4-biphenyl-thiophene (PPTPP) on the dielectrics muscovite and on phlogopite mica.

Results and Discussion

Muscovite Mica. Deposition of a layer of a few nanometers nominal thickness of PPTPP on muscovite mica (001) leads to three types of aggregates, shown exemplary in Figure 1: mutually parallel needles of typically 50 nm mean height, clusters of the same mean height in between, and flat islands, only a few nanometers tall. These aggregates do not coexist on the same area in the investigated nominal thickness range, i.e., no clusters on top of needles or flat islands, etc., are found. We also note that the height distribution function for clusters is significantly wider as compared to that for fibers.

In Figure 2, atomic force microscopy (AFM) and fluorescence microscope images demonstrate the thickness dependence for PPTPP deposited on muscovite mica at an intermediate substrate temperature of $T_S = 370$ K. In the beginning, only clusters form, which aggregate with increasing nominal thickness into short, mutually parallel fibers. Around these fibers but also around the flat islands, denuded zones of up to 1 μm width exist, demonstrated by the inset in Figure 2d, very similar to the case of *p*-6P on muscovite.[21] With increasing nominal thickness *d*, the mean height of the islands and clusters remains almost constant, whereas width and particularly the length increases considerably. In Figure 2, for example, their mean length increases from 5 μm at $d = 0.3$ nm to 30 μm at $d = 7.5$ nm. Simultaneously, the mean width rises from 200 to 500 nm, whereas the mean height stays almost constant at 40−50 nm. For low coverages, the needles are almost straight, whereas for higher coverages, needles start bending, see images c and f in Figure 2.

The morphology of the deposited films also displays a pronounced temperature dependence as shown in

(28) Balzer, F.; Rubahn, H.-G. *Appl. Phys. Lett.* **2001**, *79*, 3860–3862.
(29) Frank, P.; Hernandez-Sosa, G.; Sitter, H.; Winkler, A. *Thin Solid Films* **2008**, *516*, 2939–2942.
(30) Kankate, L.; Balzer, F.; Niehus, H.; Rubahn, H.-G. Thin Solid Films **2009**, submitted.
(31) Yanagi, H.; Morikawa, T.; Hotta, S.; Yase, K. *Adv. Mater.* **2001**, *13*, 313–317.
(32) Ichikawa, M.; Yanagi, H.; Shimizu, Y.; Hotta, S.; Sugunuma, N.; Koyama, T.; Taniguchi, Y. *Adv. Mater.* **2002**, *14*, 1272–1275.
(33) Yamao, T.; Taniguchi, Y.; Yamamoto, K.; Miki, T.; Ohira, T.; Hotta, S. *Jpn. J. Appl. Phys.* **2008**, *47*, 4719–4723.
(34) Hotta, S.; Katagiri, T.; Yamao, T.; Shimizu, K.; Yanagi, H.; Ichikawa, M.; Taniguchi, Y. *Int. J. Polym. Mater.* **2008**, *57*, 515–531.
(35) Bando, K.; Nakamura, T.; Masumoto, Y.; Sasaki, F.; Kobayashi, S.; Hotta, S. *J. Appl. Phys.* **2006**, *99*, 013518.
(36) Sasaki, F.; Kobayashi, S.; Haraichi, S.; Fujiwara, S.; Bando, K.; Masumoto, Y.; Hotta, S. *Adv. Mater.* **2007**, *19*, 3653–3655.
(37) Fujiwara, S.; Bando, K.; Masumoto, Y.; Sasaki, F.; Kobayashi, S.; Haraichi, S.; Hotta, S. *Appl. Phys. Lett.* **2007**, *91*, 021104.
(38) Hotta, S.; Goto, M. *Adv. Mater.* **2002**, *14*, 498–501.
(39) Hotta, S.; Goto, M.; Azumi, R.; Inoue, M.; Ichikawa, M.; Taniguchi, Y. *Chem. Mater.* **2004**, *16*, 237–41.
(40) Balzer, F.; Schiek, M.; Al-Shamery, K.; Lützen, A.; Rubahn, H.-G. *J. Vac. Sci. Technol., B* **2008**, *26*, 1619–1623.
(41) Schiek, M.; Balzer, F.; Al-Shamery, K.; Lützen, A.; Rubahn, H.-G. *J. Phys. Chem. C* **2009**, *113*, 9601–9608.

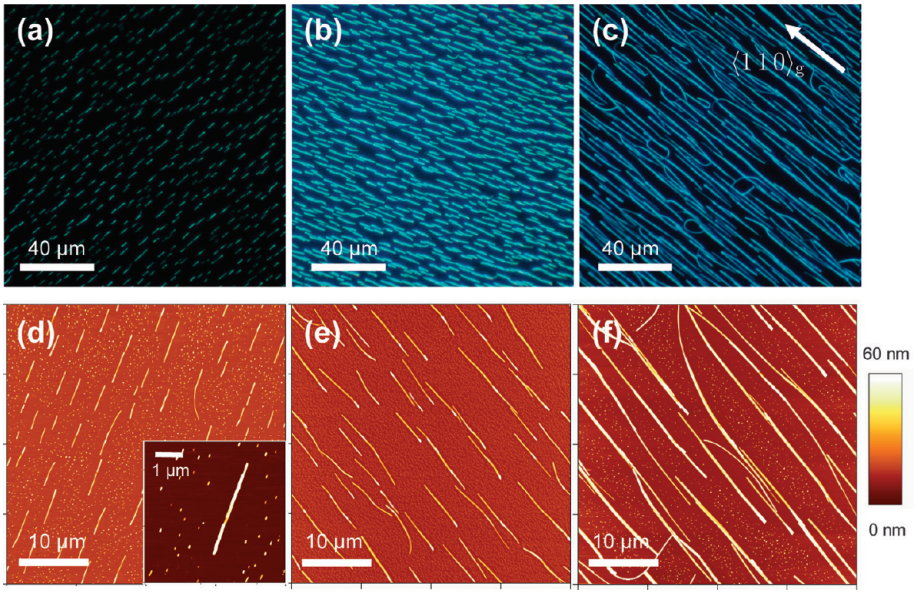

Figure 2. (a−c) Fluorescence microscope images (150 × 150 μm^2 image size) and (d−f) corresponding AFM images (each 40 × 40 μm^2 scan size with a 5 × 5 μm^2 inset in d) of PPTPP deposited on muscovite mica at a substrate temperature of T_S = 370 K. The nominal thickness increases from left to right from d = 0.3 nm via 1.5 to 7.5 nm. The direction of the needles is along a muscovite ⟨110⟩ direction, see the arrow in c.

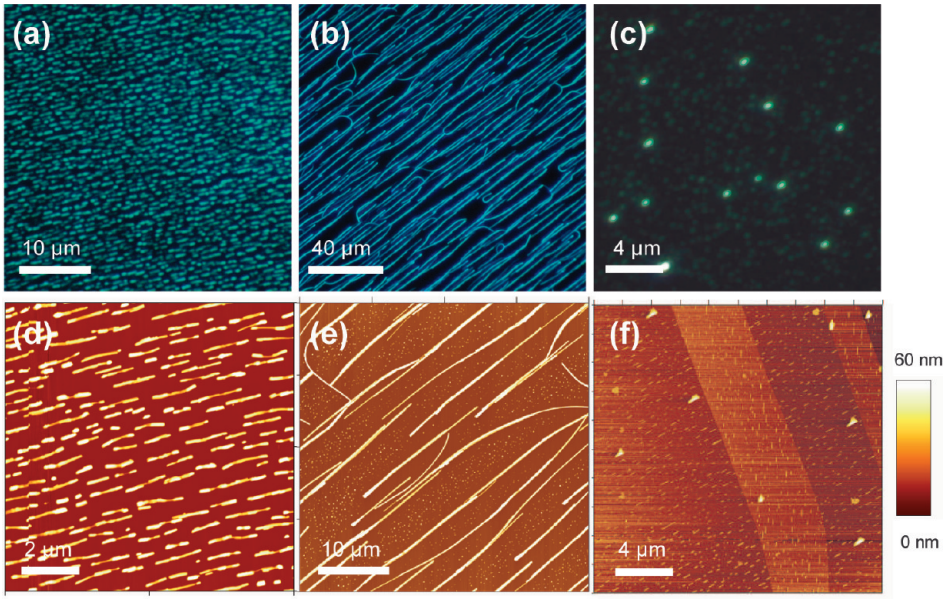

Figure 3. Fluorescence microscope images ((a) 40 × 40 μm^2, (b) 150 × 150 μm^2, and (c) 20 × 20 μm^2) and corresponding AFM images ((d) 10 × 10 μm^2, (e) 40 × 40 μm^2, and (f) 20 × 20 μm^2) of PPTPP deposited on muscovite mica at substrate temperatures (from left to right) of T_S = 293, 370, and 420 K. The nominal thickness for all images is 7.5 nm. In f, four 1 nm tall cleavage steps for the muscovite surface run diagonally through the image, separating two different needle directions.

Figure 3. For deposition at room temperature, only short needles grow, forming a dense needle film. Almost no clusters are found, because the denuded zones between the needles overlap. Increasing T_S increases the length of the needles up to more than 100 μm but decreases their number density, until a temperature of approximately 400 K is reached. Then, only short needles of a few hundred nanometers length, about 10 nm height and 70 nm width, or clusters together with few large crystallites (400 nm tall, 1 μm long) form. The flat islands are seen only occasionally on the surface, and then mostly for larger nominal thicknesses.

Both muscovite ($K_2Al_4(Si_6Al_2O_{20})(OH)_4$) and phlogopite ($KMg_3(Si_3AlO_{10})(OH)_2$) mica possess a quasi-hexagonal surface structure; the surface lattice constants are almost identical. For the bulk the unit cells are monoclinic, the lattice constants being a = 5.204 Å, b = 9.018 Å, and c = 20.073 Å with γ = 95.82° for muscovite,[42] and a = 5.332 Å, b = 9.236 Å, and c = 10.217 Å with γ = 99.98°[43] for phlogopite. A cartoon of the mica surface is presented in Figure 5b: the surface is composed of silicon

(42) Knurr, R.; Bailey, S. *Clays Clay Miner*. **1986**, *34*, 7–16.
(43) Kuwahara, Y. *Phys. Chem. Miner*. **2001**, *28*, 1–8.

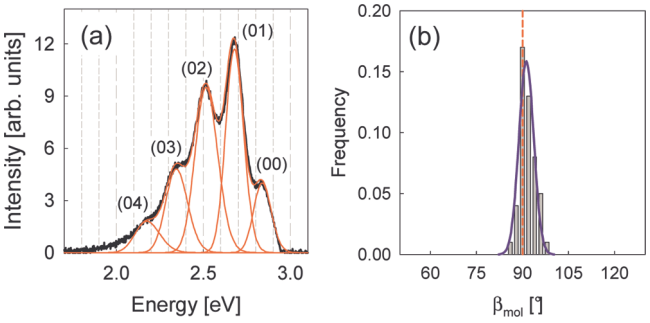

Figure 4. (a) Measured fluorescence spectrum of PPTPP on muscovite after unpolarized excitation with UV light of energy $E_{exc} = 3.4$ eV under normal incidence. Pairs (00), (01), etc., mark the different vibronic transitions. The solid lines resemble Gaussians, which fit the experimental spectrum. (b) From polarized fluorescence measurements on several PPTPP needles, the relative angle between the maximum in fluorescence and the (local) long fiber axis $\beta_{mol} \approx 90°$ is deduced.

oxide and aluminum oxide tetrahedra together with potassium cations. Note that during cleavage, half of the potassium ions remain statistically distributed on the surface,[44−46] whereas in Figure 5, a full layer of K^+ is shown. Locally, even negatively charged surface areas might exist.[47,48] The crystallographic directions of the mica substrates are obtained by the Schlagfigur technique.[21,49,50]

Two needle orientations are realized on the muscovite surface, featuring an angle of 120° in between. In Figure 3f, this is demonstrated for the high-temperature case. Obviously, the two needle directions are directly related to different muscovite mica cleavage faces. A single cleavage step of 1 nm height changes the orientation of the needles. The needle orientations are along either [110] or [1$\bar{1}$0], but never along [100]. On muscovite mica for the case of the most common $2M_1$ polytype, the two ⟨110⟩ directions differ from the [100] direction. Along one of the ⟨110⟩ directions, grooves exist.[51,52] These grooves change direction by 120° back and forth from one cleavage face to the next, i.e., for an odd number of 1 nm tall steps in between, the direction is changed; for an even number, it is not. In the following, the grooved ⟨110⟩ direction will be identified by an index "g", the nongrooved one by "ng": $\langle 110\rangle_g$ and $\langle 110\rangle_{ng}$. Connected to the grooves are electric fields on the surface that are approximately perpendicular to the groove direction[44] and are supposed to align polarizable molecules or molecules with an electric moment on the surface.

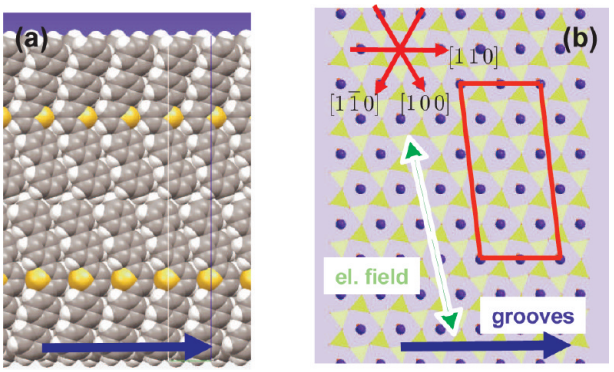

Figure 5. (a) Model for the arrangement of PPTPP molecules within a single fiber. The blue arrow depicts the fiber direction. (b) In the same scale as in a, the underlying muscovite mica surface is sketched, together with the unit cell for the wetting layer (red line), the direction of the grooves (blue arrow), and a single electric field direction (green arrow) almost perpendicular to the groove direction. SiO_4/AlO_4 tetrahedra are represented by yellow triangles, K^+ ions by blue dots.

The samples emit blue-green light after excitation with UV light at 365 nm.[31,53] The main source of fluorescence are the needles. Clusters emit less light, but mainly because of their smaller volume as compared to a needle. Emission from the flat islands is more than an order of magnitude lower than emission from the needles. It is well-known that the transition dipole moment along the long molecules axis is more than 30 times larger than the ones in the *ab* plane.[33] This, together with the observed step heights and an existing phase contrast in AFM images, suggest that the flat islands consist of upright molecules, not lying ones.

In Figure 4a, a typical fluorescence spectrum after UV irradiation under normal incidence is shown. Several excitonic peaks are resolved, being fit by five Gaussians. The peaks are situated at 2.838, 2.678, 2.515, 2.344, and 2.176 eV, agreeing with spectra known from the literature.[31] The peak at 2.678 eV has been identified as the (01) vibronic transition.[35,54]

The peak positions do not depend on process parameters such as T_S or d, whereas their relative intensities (Huang−Rhys factor) change. This results in films appearing either more bluish or more greenish. The emitted light from the fibers is polarized and can be fit by Malus' law. In Figure 4b, a histogram of measured angles β_{mol} of the maximum in fluorescence light with respect to the long needle axis is plotted, measured for several individual needles. The distribution peaks at $\beta_{mol} \approx 90°$, taking into account errors from, for example, depolarization by the dichroic mirror in the optical microscope. The transition dipole moment for the HOMO−LUMO transition is along the long molecular axis connecting the two outermost carbon atoms.[55] Hence the long molecular axis is oriented (at least on average) perpendicularly (±5°) to the long needle axis. This even holds

(44) Müller, K.; Chang, C. *Surf. Sci.* **1969**, *14*, 39–51.
(45) Odelius, M.; Bernasconi, M.; Parrinello, M. *Phys. Rev. Lett.* **1997**, *78*, 2855–2858.
(46) Campbell, P.; Sinnamon, L.; Thompson, C.; Walmsley, D. *Surf. Sci.* **1998**, *410*, L768–L772.
(47) Distler, G.; Kortukova, E.; Kobzareva, S. *Kristall. Tech.* **1973**, *8*, 67–75.
(48) Higginbotham, I.; Williams, R.; McEvoy, A. *J. Phys. D* **1975**, *8*, 1033–1043.
(49) *Pohls Einführung in die Physik 2: Elektrizitätslehre und Optik*, 22nd ed.; Lüders, K., Pohl, R., Eds.; Springer-Verlag: Berlin, 2005.
(50) Jerome, B.; Shen, Y. *Phys. Rev. E* **1993**, *48*, 4556–4574.
(51) Griffen, D. *Silicate Crystal Chemistry*; Oxford University Press, New York, 1992.
(52) Kuwahara, Y. *Phys. Chem. Miner.* **1999**, *26*, 198–205.
(53) Yamao, T.; Ota, S.; Miki, T.; Hotta, S.; Azumi, R. *Thin Solid Films* **2008**, *516*, 2527–2531.
(54) Yanagi, H.; Yoshiki, A. *Appl. Phys. Lett.* **2004**, *84*, 4783–4785.
(55) Bando, K.; Nakamura, T.; Fujiwara, S.; Masumoto, Y.; Sasaki, F.; Kobayashi, S.; Shimoi, Y.; Hotta, S. *Phys. Rev. B* **2008**, *77*, 045205.

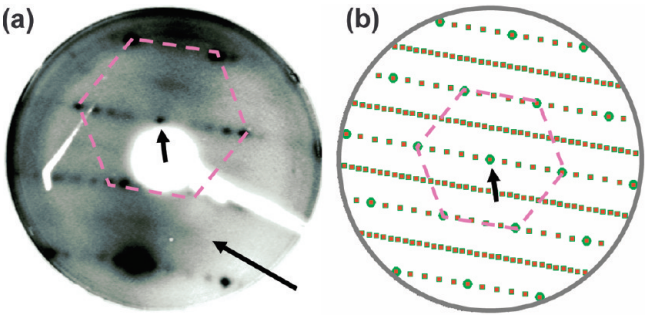

Figure 6. (a) LEED pattern from PPTPP on muscovite mica, taken at an electron energy of E_{el} = 62 eV. Superstructure spots exist in addition to the hexagonal spots from the muscovite surface. The sample has been tilted so that the specular reflection is visible (short arrow). The long arrow points to one of the faint lines in between the lines of spots. (b) Reciprocal lattice in which all the experimentally observed spots are reproduced. Circles represent diffraction spots from the muscovite substrate, squares spots from the organic overlayer. Here the specular reflection is set in the center (short arrow). In both a and b, the hexagonal diffraction pattern from the substrate is emphasized by a dashed line.

for the bent parts of needles, which appear at higher nominal thicknesses.

For PPTPP grown on KCl previous measurements have revealed lying molecules with bulk structure[56] and either the (100) or the (010) face parallel to the substrate.[31] Assuming a similar bulk packing of the molecules within the needles, molecules would arrange as shown in the sketch in Figure 5a. Here, the PPTPP (100) face as contact face is shown for simplicity, but other contact faces with slightly different tilt angles with respect to the surface normal or another polymorph cannot be ruled out by this simple optical approach. The direction perpendicular to the long molecular axis (i.e., the lamellae direction) is parallel to the grooved muscovite direction $\langle 110\rangle_g$, and the molecule's long axis close to parallel to the electric surface field.

LEED images from muscovite mica reveal a hexagonal diffraction pattern, the spots being distorted because of the electric surface fields.[57] After deposition of PPTPP the hexagonal spots are still visible, but without any distortion. Additional spots appear because of the deposited material, demonstrated in Figure 6a. The new LEED pattern is independent of both the deposited film thickness and on the substrate temperature during deposition. Both for room temperature as well as for T_S = 420 K, the pattern is visible. This suggests that, similar to the case of *p*-6P, the pattern stems neither from clusters and needles, nor from islands, but from a wetting layer of lying molecules that is initially formed. This superstructure pattern consists of spots arranged along rows, parallel to one of the sides of the muscovite hexagon. Note that in between every two well-resolved lines of spots, a rather faint additional line exists that is not resolved into individual diffraction spots.

In Figure 6b, all the experimentally obtained LEED spots are reproduced assuming a superstructure matrix

$$C = \begin{pmatrix} 2 & 0 \\ 2 & 5 \end{pmatrix}$$

for a hexagonal muscovite surface unit cell ($a = b$ = 5.204 Å, γ = 120°), suggesting a commensurate overlayer.[58] The corresponding surface unit cell with axes of length 10.4 and 22.67 Å, and with an angle of 96.6° in between, is drawn as a red parallelogram in Figure 5b. The direction of the short unit cell axis is along the long fiber axes, i.e., along $\langle 110\rangle_g$. The reciprocal lattice in Figure 6b then results from two domains of the wetting layer ($\langle 110\rangle_g$ as the mirror axis) within a single orientational domain of the needles. As a result the number of spots in each second row is doubled, leading to the unresolved lines in the diffraction pattern. The lengths of the PPTPP unit cell axes do not agree with the projection of the bulk unit cell such as for (100) or (010), i.e., the wetting layer is distorted. Along the long axis now only a single molecule can be placed into the unit cell, compared to two molecules for the bulk projections. Apparently the relative tilt of the molecules in between two adjacent lamellae as shown in Figure 11b, which results in a bulk *c*-axis of two molecules length, is lifted.

The formation of two domains of uniaxially aligned needles can be explained by electric field assisted epitaxy. Epitaxy forces the crystallites to grow with the lamella direction along a muscovite high symmetry (hs) direction as already sketched in Figure 5a. The electric fields select a single direction out of three possible ones via a dipole−induced dipole or dipole−quadrupole interaction with the molecules, i.e., the grooved $\langle 110\rangle$ direction.[40] PPTPP is thus more similar to the *p*-phenylenes than to the α-thiophenes. For the latter ones, not the lamellae direction but the molecules' long axes are parallel to a muscovite hs direction.[30]

For the flat islands, different step heights of 1.7 and 2.2 nm and sub-1 nm are observed. A step of 2.2 nm agrees very well with the distance of the (002) planes, i.e., upright molecules on the surface, though for a step height of 1.7 nm, the molecules have to be either tilted on the surface or broken. There seems to be no specific alignment of those islands on the muscovite surface, having a rather dendritic shape and usually being associated with already existing needles. Apparently, the needles act as nucleation seeds.

Phlogopite Mica. Phlogopite mica possesses a trioctahedral structure, in contrast to the dioctahedral muscovite. On phlogopite no uniaxial grooves exist,[43] and also no uniaxial electric surface fields. Thus, the deposition of *p*-6P on this substrate results simultaneously in three different growth directions. Obviously, only the epitaxial interaction is responsible for the orientation because no uniaxial electric fields exist. Deposition of PPTPP under the same conditions as for muscovite also leads to clusters, flat islands, and needlelike aggregates, with a similar thickness and temperature dependence, see Figures 7 and 8. The needles' mean height is identical to the case on muscovite, but the coverage of the substrate by flat islands is considerably larger. These islands start their growth later than the needles, but are not necessarily

(56) Smilgies, D.-M.; Blasini, D.; Hotta, S.; Yanagi, H. *J. Synchrotron Radiat.* **2005**, *12*, 807–811.
(57) Müller, K.; Chang, C. *Surf. Sci.* **1968**, *9*, 455–458.
(58) Hooks, D.; Fritz, T.; Ward, M. *Adv. Mater.* **2001**, *13*, 227–241.

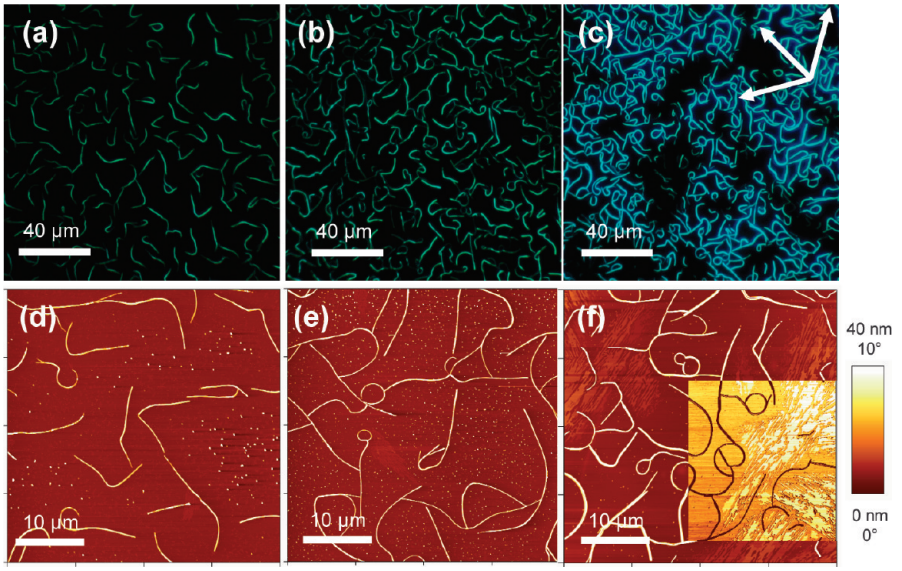

Figure 7. (a−c) Fluorescence microscope images (each 150 × 150 μm^2 image size) and (d−f) corresponding AFM images (40 × 40 μm^2 scan size) for PPTPP deposited at various thicknesses of d = 0.3, 1.5, and 6.0 nm on phlogopite mica. The deposition temperature is T_S = 340 K. The inset in f shows the phase contrast of this part of the image. In c, the three phlogopite hs directions are denoted by white arrows. Height scales for the three AFM images are 40 nm; for the inset in f, the phase scale is 10°.

nucleating at already existing needles, so needles do not serve as nucleation seeds. Because of the higher island coverage for the larger nominal thicknesses, needles can grow over flat islands, opposite to muscovite. Then, because of a decrease in surface energy,[59] their height increases to a great extent, to 100−150 nm. As already discussed above, the flat islands display a contrast in AFM phase contrast images both with respect to the fibers and to the substrate, shown in Figure 7.

The needlelike aggregates might be bent, leading eventually to the growth of rings and loops. Ring and loop formation, although resulting in up to six times taller entities, has been observed for *p*-6P deposited on water-rinsed muscovite.[60] In that case as well as for carbon covered muscovite,[27] a large number of islands from upright molecules form. Both are attributed to a reduced interaction of the molecules with the substrate.[22] Although at a first glance the PPTPP needle directions seem randomly distributed, a Fourier analysis shows that three distinct growth directions are preferred: the phlogopite hs directions [100], [110], and [$\bar{1}$10]. This becomes most apparent for deposition at room temperature as demonstrated in images a and d in Figure 8. At higher growth temperatures and/or larger nominal thicknesses, needles tend to grow in a bent shape. On muscovite, this trend is observed, too, but to a much lesser extent, compare Figure 2f and Figure 3e. Needles form only until a maximal deposition temperature. At this deposition rate for T_S above approximately 360 K, 40 K less than for muscovite, again only small clusters or short needles form, images c and f in Figure 8.

The polarization properties of the needles on phlogopite are rather similar to the ones on muscovite. The maximum in fluorescence is perpendicular to the (local) long needle axis, suggesting that the crystal structure is similar or even identical. But opposite to the case on muscovite, LEED does show only a very weak pattern from a molecular overlayer, see the schematic in Figure 9a. Green discs correspond to diffraction spots from the hexagonal phlogopite surface, blue squares to spots from the molecular overlayer. The pattern is fundamentally different from the pattern of the wetting layer on muscovite. Instead of diffraction spots along a single direction now groups of spots are observed, stemming from several domains on the surface. The experimentally obtained LEED pattern can be reproduced assuming the (001) face of the bulk PPTPP to be the contact face to the substrate, having a glide plane along PPTPP [010]. For the hexagonal phlogopite surface unit cell ($a = b = 5.33$ Å, γ = 120°), this results in the superstructure matrix

$$C = \begin{pmatrix} 1 & 1.61 \\ -1 & 0.18 \end{pmatrix}$$

using the bulk crystal structure from,[61] c.f. the red diamonds in Figure 9a. Note that the crystal structure from[38] leads to almost identical results. The unit cell is rotated by 22° with respect to one of the phlogopite hs directions, see Figure 9b, where the surface lattice of the phlogopite substrate (dashed lines) together with a single domain of the deduced PPTPP lattice (red diamonds) and the PPTPP unit cell (solid lines) is sketched. Such an angle of 22° in between PPTPP [100] and, e.g., phlogopite [100] results in the parallelism of PPTPP [110] with phlogopite [110]. All lattice points from the overlayer coincide with

(59) Balzer, F.; Kankate, L.; Niehus, H.; Frese, R.; Maibohm, C.; Rubahn, H.-G. *Nanotechnology* **2006**, *17*, 984–991.
(60) Balzer, F.; Beermann, J.; Bozhevolnyi, S.; Simonsen, A.; Rubahn, H.-G. *Nano Lett.* **2003**, *3*, 1311–1314.
(61) Dingemans, T.; Murthy, N.; Samulski, E. *J. Phys. Chem. B* **2001**, *105*, 8845–8860.

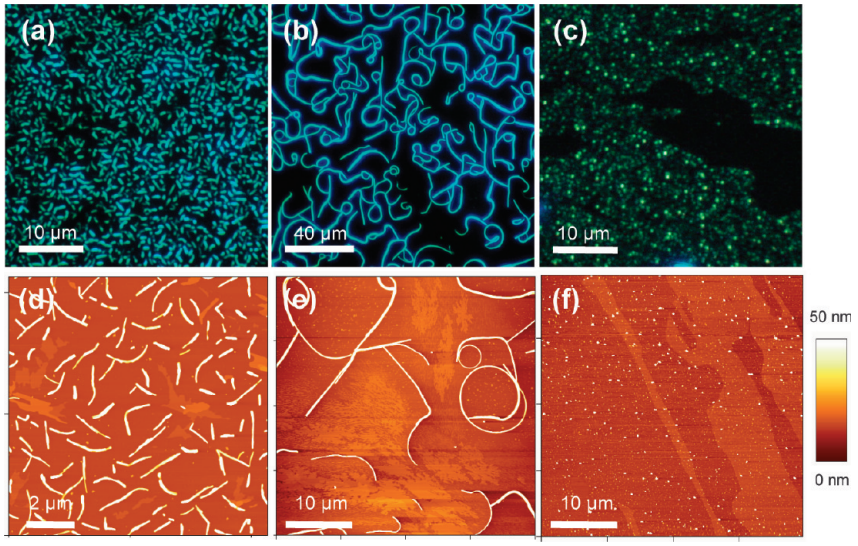

Figure 8. Fluorescence microscope images ((a, c) $40 \times 40\,\mu m^2$, (b) $150 \times 150\,\mu m^2$) and corresponding AFM images ((d) $10 \times 10\,\mu m^2$, (e, f) $40 \times 40\,\mu m^2$) for PPTPP deposited on phlogopite mica at different substrate temperatures: $T_S = 293$, 360, and 370 K from left to right. The nominal thickness is about $d = 6$ nm in all cases.

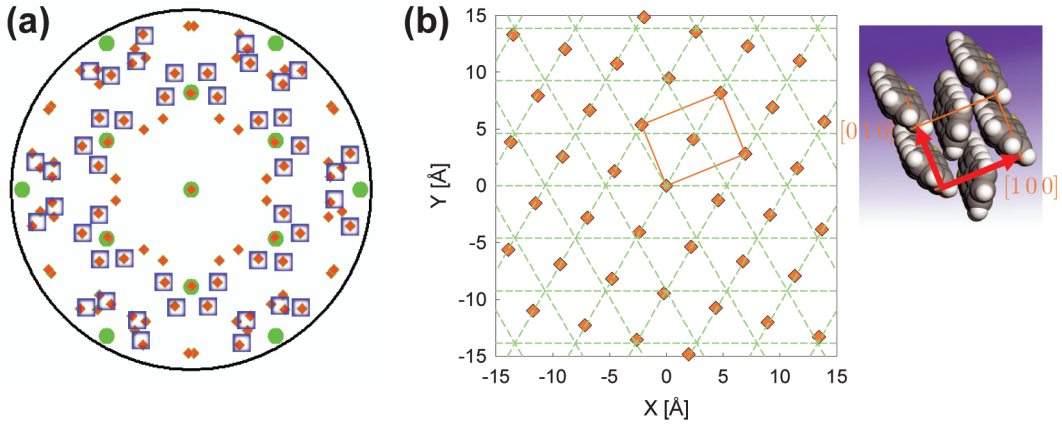

Figure 9. (a) Schematic LEED pattern for PPTPP deposited on phlogopite mica. A very weak superstructure (blue squares) is visible, in addition to the hexagonal spots from the phlogopite substrate (green discs). The red diamonds represent the reciprocal lattice from the proposed structure. (b) Model for the orientation of the epitaxial layer of upright PPTPP molecules. Dashed green lines represent the surface lattice of phlogopite, red diamonds the lattice (plus the additional molecule in the center, c.f. the inset) from a single PPTPP domain. The PPTPP [100] direction is rotated by 22° with respect to the horizontal.

lattice lines from the substrate, the overlayer forms a point-on-line coincidence lattice.[62] Altogether twelve different domains are possible on the surface, leading to six different diffraction patterns. The 12 inner spots from the reciprocal lattice are not found in the LEED pattern. They might be either too weak to be observed or they might be extinct because of a second glide plane, now parallel to PPTPP [100]. Step heights for the islands are, as for PPTPP on muscovite, 1.7 and 2.2 nm with sub-1 nm steps. These differences do not manifest themselves in different LEED patterns, but are rather typical for thiophenes.[30] A geometrical analysis using EpiCalc[63] predicts the same orientations for upright bulk PPTPP molecules on phlogopite as observed experimentally. On muscovite mica with its slightly shorter lattice constant, such a geometrical analysis does not lead to preferred directions for upright molecules, because now the lattice points from the overlayer do not coincide with substrate lattice lines.

In addition to the needles, the flat islands also obey preferred growth directions, see Figure 10. The islands are elongated and possess long straight edges as demonstrated in Figure 10a, their elongation being along a number of different crystallographic directions. In Figure 10b, it is shown that along 180°, nine different orientations are present: six close to the substrate hs directions, three in between those directions. The six directions close to the hs directions are along the proposed PPTPP [010] directions from Figure 9, i.e., at ± 8° with respect to the hs directions (dot dashed lines in Figure 10b). From this, we conclude that the edges of these islands are the PPTPP [010] directions. The additional three orientations are centered in between the hs directions, i.e., close to but not exactly along PPTPP [100]. Within experimental error, no anisotropy between the average length of the two types of edges is observed.

(62) Mannsfeld, S.; Fritz, T. *Phys. Rev. B* **2005**, *71*, 235405.
(63) Hillier, A.; Ward, M. *Phys. Rev. B* **1996**, *54*, 14037–14051.

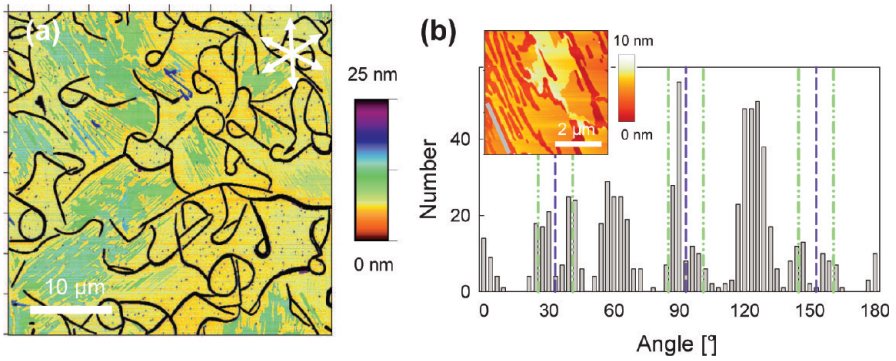

Figure 10. (a) $40 \times 40\ \mu m^2$ AFM image of PPTPP islands and needlelike entities on phlogopite mica. The white arrows represent the three phlogopite hs directions. (b) Histogram of the directions of the flat islands' long sides. In the AFM image in the inset, such a direction is marked by a gray line. The dashed vertical lines label the phlogopite hs directions, the dot-dashed ones the PPTPP [010] directions from Figure 9 for all possible domains.

The coverage by flat islands for deposition under similar conditions is larger for phlogopite than for muscovite. From this and from the bending of needles, it is concluded that the interaction with the substrate is smaller for the case of phlogopite as compared to muscovite.[64] However, for *p*-6P on muscovite and phlogopite, no such differences are observed except for the number of needle orientations. In both cases, only very few islands are generated from upright molecules, although a similar coincidence lattice as for PPTPP would be possible on phlogopite. For a better understanding, the surface energies of the different molecular faces together with the substrate surface energies and the substrate/molecule interaction have to be known. Whereas surface energies have been measured for mica[65,66] and have been calculated for the *p*-phenylenes and α-thiophenes,[64] they are not yet accessible for the co-oligomers.

Conclusions

In this article, we demonstrate via extensive surface growth investigations that after vacuum sublimation on the basal surfaces of muscovite and phlogopite mica the PPTPP molecules form aggregates such as fibers, clusters, and islands. The observed overall growth mechanism of the fibers from conjugated organic molecules seems to be quite universal for the muscovite mica substrates. First a wetting layer from lying molecules is formed. On this wetting layer, clusters from lying molecules grow, which finally aggregate into fibers made of lying molecules. Islands made of upright molecules nucleate at already existing needles. Morphology parameters such as widths and heights of clusters and fibers are similar, but the orientations of the fibers differ for different molecules. Their growth directions are determined by two driving forces: epitaxy and alignment due to surface electric fields. Regarding the realized needle orientations PPTPP behaves more like a *p*-phenylene: needles grow along a single substrate hs direction as opposed to the thiophenes α-4T and α-6T and the co-oligomers PPTTPP and TTPPTT, whose needle growth directions are considerably off the hs directions and where several simultaneous needle directions are realized.[40] This opens up an easy way to design needle films with, e.g., specific morphological as well as light-emitting properties.

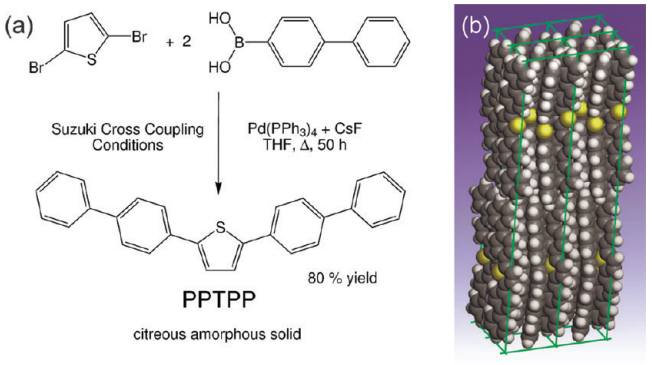

Figure 11. (a) Synthesis of PPTPP. (b) Crystal structure for bulk PPTPP crystallites from ref 61. Four unit cells are drawn.

Experimental Section

Synthesis. Under an argon atmosphere, 484 mg (2.0 mmol, 0.22 mL) of 2,5-dibromo thiophene, 832 mg (4.2 mmol, 2.1 equivalents) of 4-biphenyl boronic acid, 1.200 g (8.0 mmol, 4 equivalents) of cesium fluoride, and 115 mg (0.10 mmol, 5 mol %) of $[Pd(PPh_3)_4]$ were dissolved in 80 mL of abs. THF and refluxed for 50 h. After being cooled to room temperature, the reaction mixture was diluted with petrol ether, and the precipitate was filtered off and washed with ethyl acetate, water, and dichloromethane to give 615 mg (1.58 mmol, 80%) of a citreous amorphous solid, c.f. Figure 11a.

MS (EI): m/z 388.1 (M^+), 194.1 (M^{2+}).

HR-MS (EI): calcd for $C_{28}H_{20}S$, 388.1286; found, 388.1282.

UVvis (dichloromethane): $\lambda_{max} = 356$ nm.

Fluorescence (dichloromethane): $\lambda_{max} = 413$ nm.

Elemental anal. Calcd for $C_{28}H_{20}S + 0.5\,CH_2Cl_2$: C, 79.42; H, 4.91; S, 7.44. Found: C, 79.40; H, 5.07; S, 7.80.

The crystal structure of bulk PPTPP crystals (or "BP1T") has been determined by two different groups.[38,61] In both cases, a monoclinic unit cell ($P2_1/n$ symmetry) has been found, hosting four molecules in a herringbone packing. Unit-cell axes agree well. Either $a = 7.4972$ Å, $b = 5.7929$ Å, $c = 43.6290$ Å, and $\beta = 93.342°$ or $a = 7.608$ Å, $b = 5.8219$ Å, $c = 43.76$ Å, and $\beta = 93.51°$ have been found. That way, (002) planes have a distance of ~2.18 nm. Four unit cells from ref 61 are shown in Figure 11b.

(64) Nabok, D.; Puschnig, P.; Ambrosch-Draxl, C. *Phys. Rev. B* **2008**, *77*, 245316.
(65) Gutshall, P.; Phillips, J.; Bryant, P.; Cole, G. *J. Vac. Sci. Technol.* **1971**, *8*, 85–87.
(66) Christenson, H. *J. Phys. Chem.* **1993**, *97*, 12034–12041.

Film Deposition and Characterization. Muscovite mica (Structure Probe, Inc., West Chester, PA) and phlogopite mica (Segliwa, Wiesbaden, Germany) are cleaved in air and are introduced immediately into a high vacuum chamber with a base pressure of $p \approx 2 \times 10^{-8}$ mbar. The organic molecules are deposited from a home-built Knudsen cell onto the corresponding substrate after outgassing just below the sublimation temperature for a few hours to remove contaminants.

Samples are characterized by the nominal thickness d of deposited material, i.e., the thickness measured by a water cooled quartz microbalance (Inficon XTC/2), positioned close to the sample. Especially for high substrate temperatures, the integrated thickness of the organic molecules on the surface is considerably smaller because of the decreasing sticking factor. The error in determining relative nominal thicknesses and deposition rates is rather small, whereas the absolute values might be wrong by a factor of 2, as estimated from AFM images. Typical deposition rates are 0.02 nm/s − 0.03 nm/s. In situ, the grown thin films are characterized by low-energy electron diffraction (MCP-LEED, Omicron). Ex situ, the samples are investigated by polarized fluorescence microscopy (excitation with light from a high-pressure Hg lamp, $\lambda_{exc} = 365$ nm) and by atomic force microscopy in intermittent contact mode (JPK NanoWizard). For the AFM measurements, highly doped Silicon tips (Pointprobe NCH and NCL from NanoWorld) shaped like a polygon base pyramid and with a tip radius of less than 10 nm are used. Images consist of 512 × 512 pixels, typical scanning speeds are less than 5 μm/s. Note that all quoted numbers regarding widths, heights, and lengths are measured values that have not been tip-corrected.

Acknowledgment. The authors are grateful to the Danish research agencies FNU and FTP as well as the Danish Advanced Technologies Trust for supporting this work by various grants. A.L. thanks the German research foundation DFG for financial support.